MR Imaging of Scrotum

Athina C. Tsili, MD[a],*, Dimitrios Giannakis, MD[b],
Anastasios Sylakos, MD[b], Alexandra Ntorkou, MD[c],
Nikolaos Sofikitis, MD[b], Maria I. Argyropoulou, MD[a]

KEYWORDS

- Magnetic resonance • Imaging • Testis • Scrotum • Testicular carcinoma

KEY POINTS

- Magnetic resonance (MR) imaging of the scrotum represents a valuable supplemental diagnostic tool in the investigation of scrotal diseases.
- The technique is particularly recommended in cases of inconclusive or nondiagnostic sonographic findings.
- MR imaging of the scrotum with respect to lesion location, morphology, and tissue characterization provides important information in the presurgical work-up of scrotal masses, improving patient care and decreasing the number of unnecessary surgical explorations.
- The technique performs well in the localization of a scrotal mass, in the differentiation of paratesticular masses, in the distinction between benign from malignant intratesticular lesions, and in the evaluation of the local extent of the disease in cases of testicular carcinomas.

INTRODUCTION

Imaging has an important role in the investigation of scrotal diseases, although clinical examination represents the primary method for the evaluation of scrotal abnormalities. Sonography currently remains the modality of choice in the initial assessment of scrotal lesions.[1–8] It is easily performed, widely available, inexpensive, and has been shown to be highly sensitive in the identification of scrotal masses.[1–8] However, a confident characterization of the nature of intratesticular and paratesticular masses is not always possible, based on sonographic findings only. Magnetic resonance (MR) imaging of the scrotum has been proposed as an alternative imaging technique for the evaluation of scrotal diseases.[9–42] It is a useful diagnostic tool for the morphologic assessment and tissue characterization in the work-up of scrotal masses and reduces the need for diagnostic surgical explorations of the scrotum. The advantages of MR imaging include simultaneous imaging of both testicles, paratesticular spaces, and spermatic cords; adequate anatomic information; satisfactory tissue contrast; and functional information.[9–42] MR imaging may be a valuable problem-solving tool in the assessment of scrotal diseases when sonographic findings are equivocal or inconsistent with the clinical findings. Serra and colleagues[16] reported that MR imaging of the scrotum, when performed after inconclusive ultrasound examination, may be diagnostic and cost-effective, although in this study it was required only in 1.4% of cases.

Determining the accurate location of a scrotal mass, whether intratesticular or paratesticular, is important to ensure adequate treatment planning. Most paratesticular masses are benign; therefore,

radical orchiectomy may be obviated.[13,14,43–50] MR imaging of the scrotum has been proved highly accurate in the differentiation of extratesticular from intratesticular disease, being superior to sonography especially in cases when the scrotum is markedly enlarged. MR imaging findings with respect to tumor location, morphologic features, and tissue characterization can aid in narrowing the differential diagnosis in cases of paratesticular masses.[13,14,43–50]

Although most intratesticular masses are malignant, a possible diagnosis of various benign intratesticular entities, including dilatation of rete testis, epidermoid cyst, fibrosis, orchitis, infarction, hematoma, and hemorrhagic necrosis, based on MR features may improve patient care and decrease the number of unnecessary radical surgical procedures.[9–12,17,51–57] In these cases, follow-up, lesion biopsy, tumor enucleation, and testis-sparing surgery (TSS) may be justified. MR imaging of the testicles may provide important information in the preoperative characterization of the histologic nature of various intratesticular mass lesions in terms of morphologic information and by showing the presence of fat, fibrous tissue, fluid, and solid contrast-enhancing tissue within the masses.[9–12,17,51–57]

According to the current guidelines, radical orchiectomy remains the treatment of choice for testis neoplasms of malignant and unknown origin.[58–61] Nevertheless, in the last years the management of testicular tumors has started to change in favor of conservative surgery.[58–61] The widespread use of sonography has led to a marked increase in the number of incidentally detected, small-sized testicular mass lesions, most of which have been proved to be benign. TSS has recently been proposed as an alternative option in selected cases, namely, in small malignant germ cell tumors (GCTs) arising in both or in solitary testes, coupled with local adjuvant radiotherapy and in small Leydig cell tumors, with elective indications (healthy contralateral testes), provided that pathology fails to reveal aggressive features.[58–61] TSS is also an option in small sonographically detected, nonpalpable tumors provided that histology excludes malignancy (the incidence of benign pathology is reported at approximately 80% in these cases).[58–61]

Accurate preoperative imaging evaluation of the local stage of disease is mandatory in the care of patients who are candidates for TSS. MR imaging of the scrotum performs well in the evaluation of the local extent of testicular carcinomas.[17] Moreover, MR imaging findings can be closely correlated with the histologic characteristics of testicular neoplasms, providing a preoperative classification of the histologic type of testicular tumors.[18,34]

MR IMAGING PROTOCOL

MR imaging of the scrotum is performed with the use of a pelvic phased array coil or a surface coil. Patients are examined in the supine position, with the testes placed at a similar distance from the coil, usually by means of a towel placed beneath the testis and the penis draped on the anterior abdominal wall.

The MR imaging protocol should include

1. Thin-section spin-echo T1-weighted images in the transverse plane should be included. These images provide information about scrotal anatomy and demonstrate hyperintense lesions.
2. Axial fat-suppressed T1-weighted sequences are repeated when a lesion with high T1 signal intensity is detected.
3. Thin-section fast spin-echo T2-weighted images in 2 or 3 planes should be included, including the transverse plane and the coronal and/or the sagittal plane. These images are best for lesion detection, localization, and characterization. On the coronal plane, a comparative evaluation of both testes, the paratesticular spaces, and the spermatic cords is possible.

Dynamic contrast-enhanced (DCE) subtracted MR imaging, diffusion-weighted imaging (DWI), and MR spectroscopy (MRS) have recently added important diagnostic information in the investigation of scrotal diseases.[62–80] DCE MR imaging provides information regarding the characteristics of microvasculature of testicular carcinomas and assesses tumor angiogenesis.[81–83] In malignancies, DCE MR imaging typically shows rapid and intense enhancement, followed by a relatively rapid washout of the contrast medium; this was also proved for testicular carcinomas.[62–64,81–84] DCE MR imaging has been proved useful in the characterization of scrotal lesions and in the distinction between testicular torsion and trauma from other causes of acute pain.[62–69] DCE MR imaging in combination with T2- and T2*-weighted images is useful in the diagnosis of testicular torsion and in the detection of testicular necrosis.[66] A sensitivity of 100% was referred for DCE-MR imaging in diagnosing complete torsion by showing a decrease or lack of testicular perfusion.[66] The same group of researchers described the differences of testicular enhancement patterns in 42 patients with a variety of scrotal diseases.[63] They concluded that the relative percentages of peak height and mean slope based on time-signal intensity (TSI) curves may be used to differentiate

intratesticular from extratesticular diseases.[62] DCE subtracted MR imaging has also been used for the differential diagnosis between benign and malignant intratesticular lesions.[62] The progression of enhancement was classified according to the shape of the TSI curves into 3 types: type I curve, with a linear increase of contrast enhancement over the entire dynamic period, indicating a benign diagnosis; type II curve, with an initial upstroke, after which the signal intensity either plateaus or gradually increases in the late contrast-enhanced period, also suggestive of benignity; and type III curve, with an initial upstroke, followed by gradual washout of the contrast medium, indicating a diagnosis of malignancy (**Fig. 1**). The relative percentages of peak height, maximum time to peak, and mean slope were calculated to assess possible independent predictors of malignancy.[62] A significant association between the type of the TSI curve and the final diagnosis was demonstrated, and the relative percentages of maximum time to peak proved to be the most important discriminating factor in characterizing intratesticular masses.[62]

DWI is an evolving technique that can be used to improve tissue characterization when interpreted in combination with the findings of conventional MR sequences.[84–86] Lesion detection and characterization mainly depends on the extent of tissue cellularity, and increased cellularity is associated with restricted diffusion and reduced apparent diffusion coefficient (ADC) values.[84–86] A few series reported the usefulness of a high b value DWI in the detection and localization of nonpalpable undescended testes in children, when combined with conventional MR imaging data.[71,72] The researchers concluded that hypointensity of testicular parenchyma in these patients detected on all sequences, including DWI, may be related

to nonviable testis, therefore, preventing unnecessary surgical procedures.[71,72] Other studies concluded that ADC measurements may be used for the early diagnosis of testicular torsion, without the need of intravenous contrast media, reporting significantly lower mean ADC of the twisted testes than that of the normal contralateral testes because of the presence of ischemia and/or hemorrhagic necrosis.[73,74] DWI and ADC measurements have been reported to be useful in differentiating between normal, benign, and malignant scrotal contents when interpreted in combination with the conventional MR imaging.[87] By combining DWI ($b = 900$ s/mm^2) with conventional MR imaging, an accuracy of 100% has been reported in the characterization of scrotal lesions.[70]

The MR imaging protocol for the evaluation of scrotal masses is described in **Table 1**.

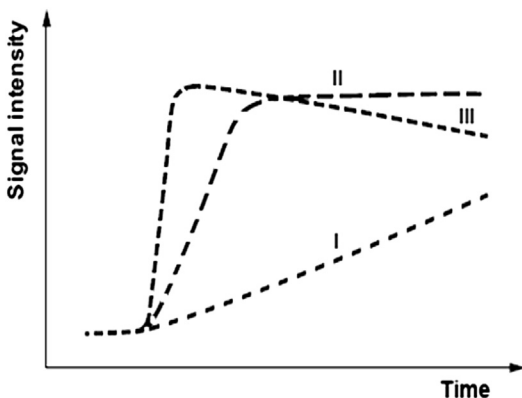Proton MRS (^{1}H-MRS) provides chemical data on tissue components and has been recently

Table 1
Suggested MR imaging protocol for imaging of the scrotum

Sequences	Parameters
Transverse spin-echo T1-weighted In cases of hyperintense lesions on T1-weighted images, repeated with fat saturation	TR/TE (ms): 500–650/ 13–15 Slice thickness (mm): 3–4 Gap (mm): 0.5 Matrix (mm): 180 × 256 FOV (mm): 240 × 270
Transverse, coronal and sagittal fast-spin echo T2-weighted	TR/TE (ms): 3900/120 Slice thickness (mm): 3–4 Gap (mm): 0.5 Matrix (mm): 180 × 256 FOV (mm): 240 × 270
Transverse DW single-shot, multi-slice spin-echo planar diffusion pulse	TR/TE (ms): 4000/115 Slice thickness (mm): 3–4 Gap (mm): 0.5 Matrix (mm): 180 × 256 FOV (mm): 240 × 270 b value (s/mm^2): 0, 900
Coronal dynamic 3D fast-field subtracted postcontrast	TR/TE (ms): 9/4.1 Slice thickness (mm): 4 Gap (mm): 0 Matrix (mm): 256 × 256 FOV (mm): 219 × 219 Flip angle: 35° Dynamic scans: 7 (every 60 s) Contrast material IV (mL/kg): 0.2

Abbreviations: 3D, 3 dimensional; FOV, field of view; IV, intravenous; TR/TE, time repetition/time echo.
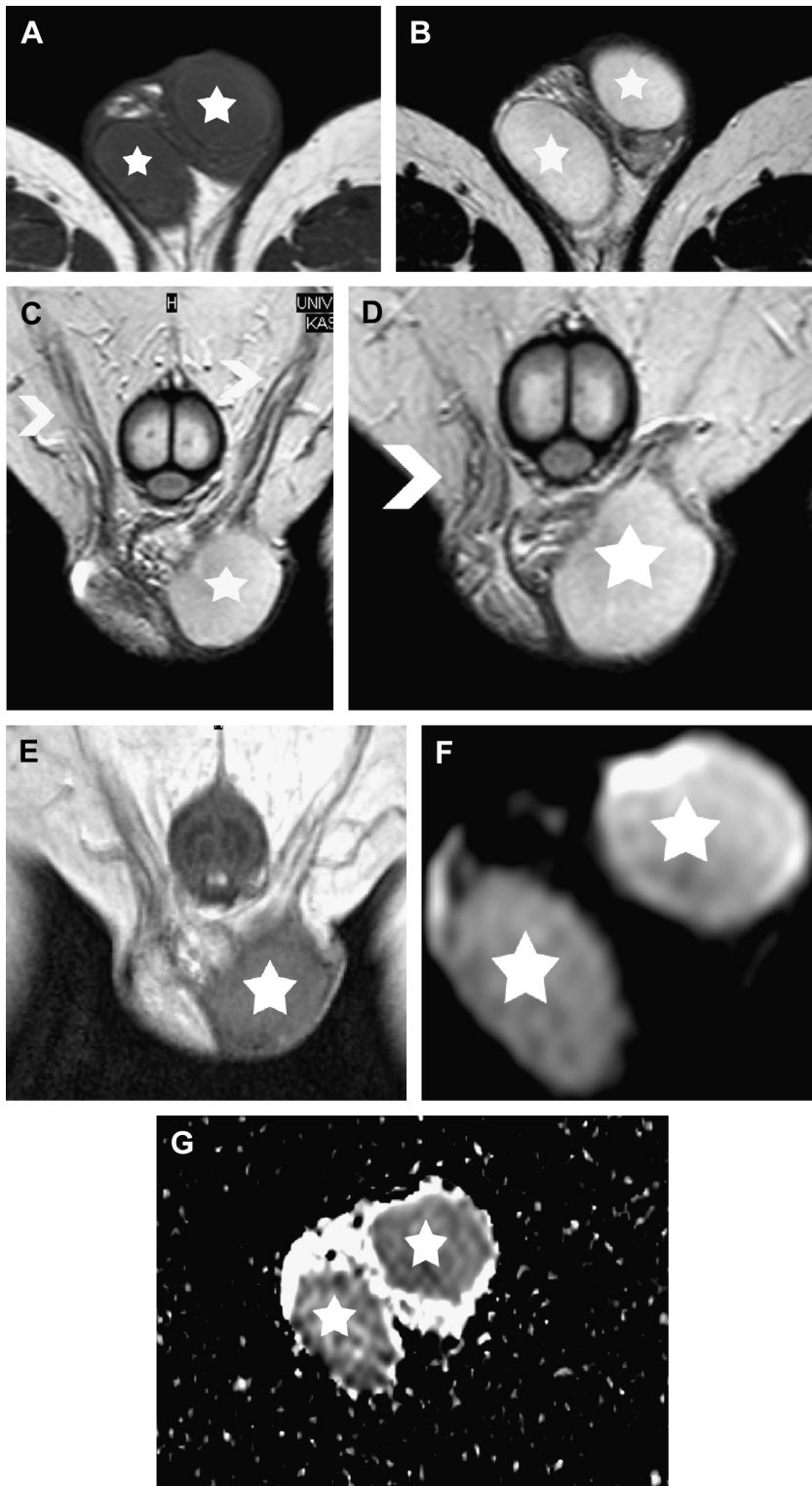

Fig. 1. The TSI curve types.

Fig. 2. Normal MR imaging examination of the scrotum in a 36-year-old man. (*A*) Transverse T1-weighted image shows normal testes (*asterisks*), with signal intensity similar to that of the surrounding muscles. (*B*) Transverse T2-weighted image. Normal testicular parenchyma (*asterisks*) appears hyperintense. The testes are surrounded by a thin hypointense halo, corresponding to tunica albuginea. (*C, D*) Coronal T2-weighted images show normal appearance of both spermatic cords (*arrowheads*). Normal left testis (*asterisk*). (*E*) Coronal DCE image depicts homogeneous enhancement of normal testicular parenchyma (*asterisk*). (*F*) Transverse DW image (b = 900 s/mm^2) depicts normal testes (*asterisks*) with high signal intensity. (*G*) The ADC values of normal testes (*asterisks*) are 1.04×10^{-3} mm^2/s (right testis) and 1.01×10^{-3} mm^2/s (left testis).

used for the study of human testes.[75–80] Firat and colleagues[75] showed differences in ^{1}H-MRS characteristics between prepubertal and postpubertal male volunteers. An increase of choline peak and a significant decrease of the lipid peak have been reported after puberty, both related to the initiation of spermatogenesis.[75] Aaronson and colleagues[76] showed a significantly high phosphocholine concentration in testes with spermatogenesis, concluding that ^{1}H-MRS may provide a noninvasive imaging tool in the investigation of male infertility.

NORMAL ANATOMY

Normal testes appear homogeneous, with signal intensity similar to that of the surrounding muscle on T1-weighted images (**Fig. 2**). The internal structure of testicular parenchyma is better appreciated on T2-weighted images. Normal testes appear hyperintense on T2-weighted sequences, although the signal intensity is less than that of fluid (see **Fig. 2**; **Fig. 3**). Thin radiating hypointense septa are often seen through parenchyma toward the mediastinum testis, which is depicted as a low-signal-intensity band in the posterior aspect of the testis. The tunica albuginea appears as a thin hypointense halo surrounding the testis. Normal testis enhances moderately and homogeneously after gadolinium administration (see **Fig. 2**E), with a gradual increase of signal intensity throughout the examination (type I curve).[62–64] This behavior is probably related to an intact blood-testis barrier.[62–64] Testicular parenchyma has been reported hyperintense and slightly hypointense on high b value DWI and ADC maps, respectively, because of the complexity in histology of normal testicular parenchyma (see **Fig. 2**F, G).[70] Densely packed seminiferous tubules, lined by a compact fibroelastic connective tissue sheath and interstitial stroma, containing fibroblasts, blood vessels, lymphatics, and the Leydig cells within normal testis, are responsible for the restricted diffusion.[12,70] ADC values of the normal testis have been previously published ($1.11 \pm 0.18 \times 10^{-3}$ mm^2/s).[70]

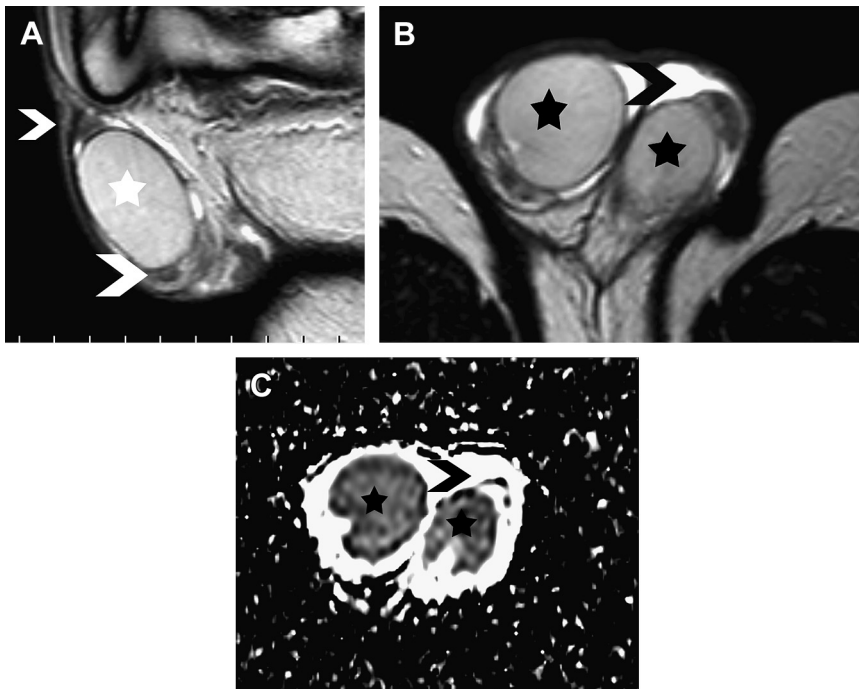The normal epididymis appears as isointense on T1- and hypointense on T2-weighted sequences,

Fig. 3. Normal findings in a 21-year-old man. (*A*) Sagittal and (*B*) transverse T2-weighted images show normal hyperintensity of both testes (*asterisks*). The left epididymis (head and tail, *arrowhead*) appears hypointense. A small amount of hydrocele is noted bilaterally. (*C*) Transverse ADC map ($b = 900$ s/mm^2) depicts hyperintensity of the left epididymal head (*arrowhead*). The ADC values of testicular parenchyma (*asterisks*) are 0.87×10^{-3} mm^2/s (right testis) and 0.92×10^{-3} mm^2/s (left testis), and the ADC value of the left epididymis is 1.69×10^{-3} mm^2/s (*arrowhead*).

respectively, and is better appreciated on sagittal T2-weighted images (see **Fig. 3**). It appears with low signal intensity on DWI, and the mean ADC is $1.39 \pm 0.14 \times 10^{-3}$ mm^2/s (see **Fig. 3**C). A small hydrocele is often seen in the scrotum and is considered a physiologic finding. The spermatic cords are better evaluated on coronal T2-weighted sequences, as hyperintense structures, because of the presence of fat, with hypointense vessels coursing through them (see **Fig. 2**C, D).

Box 1
Histologic classification of malignant testicular tumors

GCTs

  Intratubular germ cell neoplasia, unclassified

  Malignant pure GCT (showing a single cell type)

    Seminoma

    Embryonal carcinoma

    Teratoma

    Choriocarcinoma

    Yolk sac tumor

  Malignant mixed GCT (showing more than one histologic type)

    Embryonal carcinoma and teratoma with or without seminoma

    Embryonal carcinoma and yolk sac tumor with or without seminoma

    Embryonal carcinoma and seminoma

    Yolk sac tumor and teratoma with or without seminoma

    Choriocarcinoma and any other element

  Polyembryoma

Sex cord and stromal tumors

  Leydig cell tumor

  Sertoli cell tumor

  Granulosa cell tumor

  Fibroma-thecoma

Tumors with both sex cord and stromal cells and germ cells

  Gonadoblastoma

Lymphoid and hematopoietic tumors

  Lymphoma

  Leukemia

Metastases

PATHOLOGY
Intratesticular Masses

Testicular tumors

Testicular carcinoma, although representing 1.0% to 1.5% of all malignancies in men, is the most common neoplasm in boys and young adults aged 15 to 34 years old.[12,87–91] The estimated number of new cases of testicular cancer in the United States during 2013 is 7920, and deaths related to testicular cancer are estimated to occur in 370 patients.[87] Testicular cancer more often presents as a painless scrotal mass.

Testicular tumors may be subdivided into GCTs and non-GCTs (**Box 1**). Most (95%) testicular carcinomas are GCTs, arising from the germinal epithelium of the seminiferous tubules.[88–91] The GCTs are fairly evenly split between seminomas and nonseminomatous GCTs (NSGCTs). Less than 50% of malignant GCTs have a single cell type, of which roughly 50% are seminomas, seen more often during the fourth decade of life. The remaining testicular tumors have more than 1 cell

---

Table 2
Staging classification of testicular cancer and assessment of primary tumor

Stage of Primary Tumor	Extent of Primary Tumor Assessed After Radical Orchiectomy
pTx	Primary tumor cannot be assessed
pT0	No evidence of primary tumor in the testis
pTis	Intratubular germ cell neoplasia or carcinoma in situ
pT1	Tumor confined to the testis, without vascular or lymphatic invasion, with or without involvement of the epididymis or rete testis: may invade the tunica albuginea but not the tunica vaginalis
pT2	Tumor confined to the testis, with or without involvement of the epididymis or rete testis, with vascular or lymphatic invasion or extension through the tunica albuginea with invasion of the tunica vaginalis
pT3	Tumor invades the spermatic cord with or without vascular or lymphatic invasion
pT4	Tumor invades the scrotal wall with or without vascular or lymphatic invasion

type.[88–91] NSGCTs include a large group of histologically diverse neoplasms, with 4 basic types, including embryonal carcinoma, teratoma, choriocarcinoma, and yolk sac tumor. NSGCTs typically occur earlier in life, usually during the third decade.[88–91]

The local extent (T) of testicular tumors is classified according to the recommendations of the European GCC Consensus Group (EGCCCG)

and is presented in **Table 2**.[58] More than 70% of GCTs are diagnosed at an early stage.

Most non–germ cell neoplasms of the testis are derived from the cells forming the sex cords (Sertoli cells) and the interstitial stroma (Leydig cells).[1,12,88–92] These neoplasms compose approximately 4% of all testicular malignancies in adults, with a higher incidence in children (10%–30%). Although they are usually benign
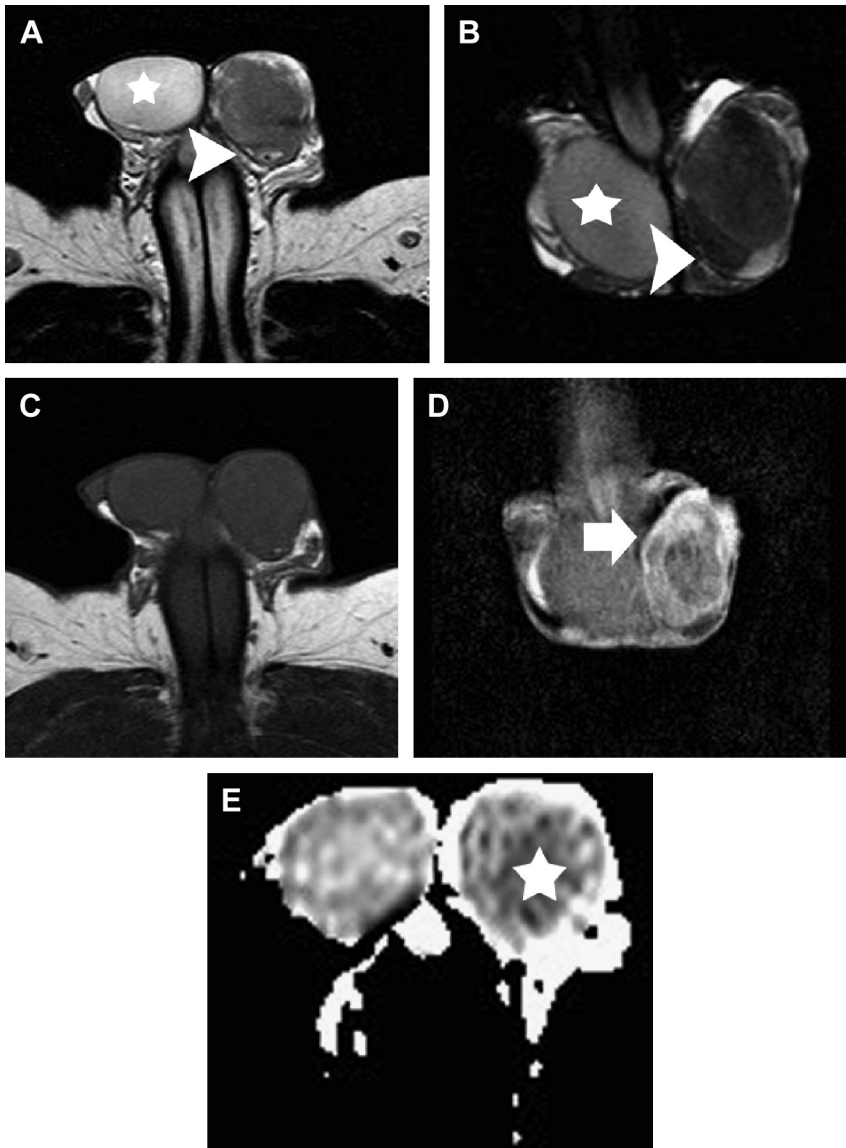

Fig. 4. Left testicular seminoma in a 27-year-old man invading the paratesticular space (pT2). (*A*) Axial and (*B*) coronal T2-weighted images show left intratesticular tumor extending into the paratesticular space (*arrowhead*). The mass is mainly homogeneous and hypointense when compared with the normal contralateral testis (*asterisk*). (*C*) Axial T1-weighted image fails to demonstrate the neoplasm. (*D*) Coronal DCE image depicts inhomogeneous tumor enhancement (*arrow*). (*E*) Transverse ADC map (b = 900 s/mm^{-2}) shows restricted tumor diffusion (*asterisk*). The ADC values of the neoplasm are 0.50×10^{-3} mm^2/s^{-1}, less than that of the normal contralateral testis (0.98×10^{-3} mm^2/s^{-1}).

(90%), the preoperative diagnosis of their nature is usually difficult.

Testicular lymphoma constitutes 1% to 9% of all testicular carcinomas but represents the most common testicular tumor in men older than 60 years. Secondary involvement of the testis in patients with an established lymphoma is much more common than primary testicular lymphoma. It is the most common bilateral testicular neoplasm, often locally invasive, typically infiltrating the epididymis, the spermatic cord, and the scrotal skin.[12,93–95] Leukemia may appear as an infiltrative epididymal-testicular mass, more often in patients with a known history of treated leukemia.[12]

MR imaging findings

Conventional MR imaging criteria used to characterize testicular malignancies include the presence of a predominantly hypointense intratesticular mass lesion on T2-weighted images when compared with the normal testis (Fig. 4) or a heterogeneous mass with variable signal intensity on T2-weighted images (Fig. 5), inhomogeneously enhancing after gadolinium administration (see Figs. 4 and 5).[12–18] All testicular neoplasms usually have similar signal intensity with the normal contralateral testis on T1-weighted sequences (see Fig. 4C). The coexistence of areas of hemorrhage and/or necrosis within the tumor (see Fig. 5; Fig. 6) as well as the extension of the neoplasm to the testicular tunicae (Fig. 7), the paratesticular space (see Fig. 4), and/or the spermatic cord (Fig. 8) are considered as secondary findings used to confirm the diagnosis of malignancy.[12–18]

Imaging features of testicular carcinomas closely correlate with gross morphology and histologic characteristics.[1,12,18,34] On pathology, classic seminomas are often homogeneously solid, lobulated masses, composed of uniform tumor cells with abundant clear cytoplasm. These cells are arranged in nests outlined by fibrous
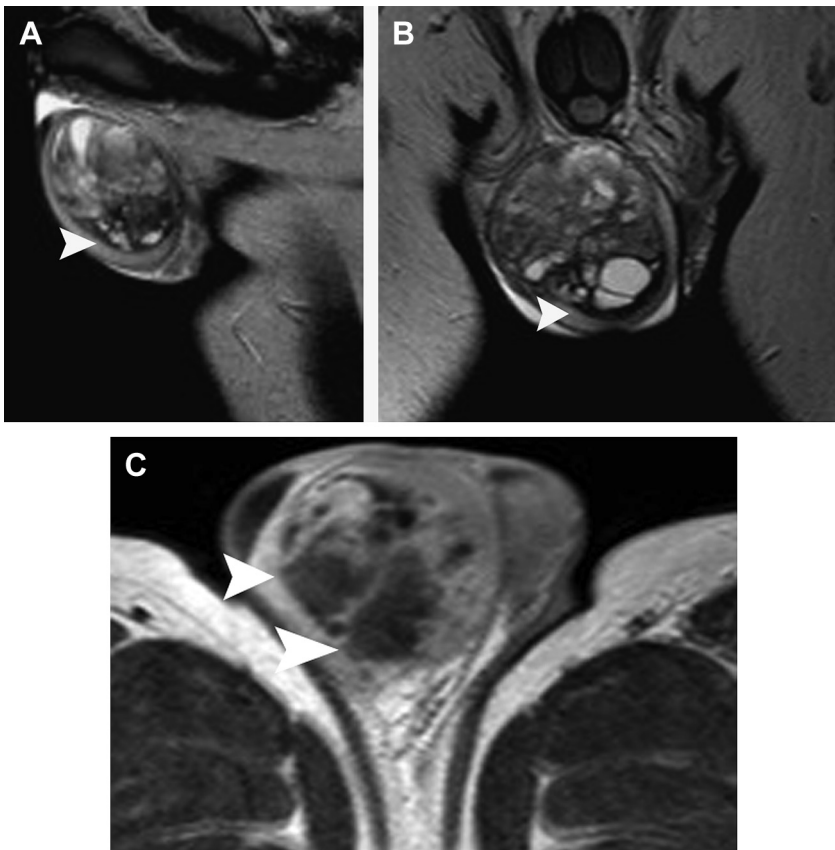

Fig. 5. Mixed germ cell tumor of the right testis in a 41-year-old man (embryonal carcinoma, yolk sac tumor, and teratoma). (A) Sagittal and (B) coronal T2-weighted images show extremely heterogeneous right intratesticular mass. The neoplasm is surrounded by a thin hypointense halo (*arrowhead*), corresponding to fibrous pseudocapsule on pathology. (C) Transverse contrast-enhanced T1-weighted image shows inhomogeneous tumor enhancement. Nonenhancing areas corresponded to areas of necrosis on histology (*arrowheads*).
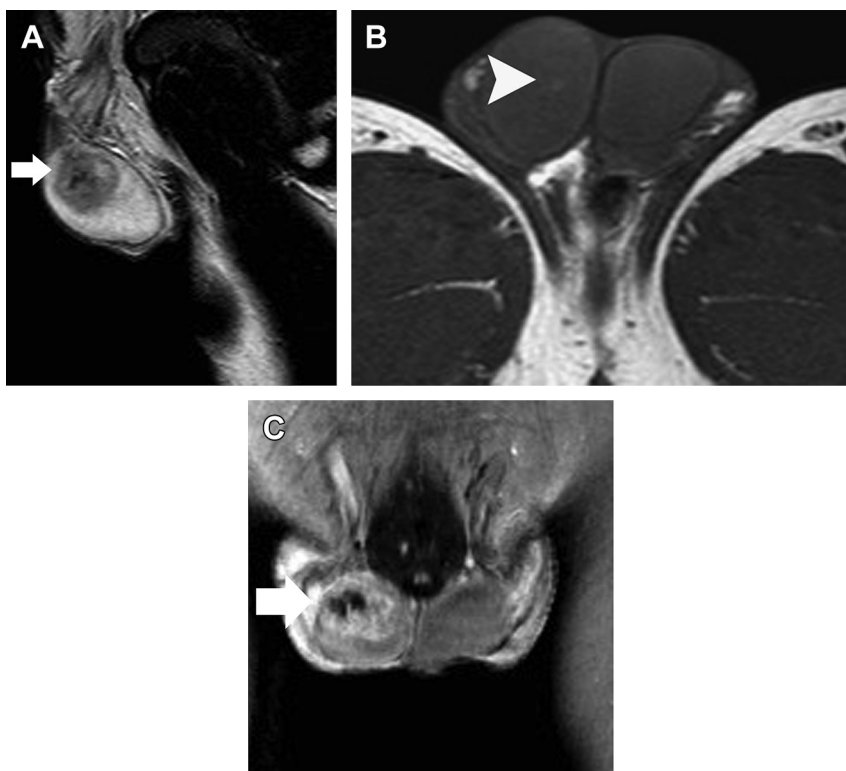
Fig. 6. Embryonal carcinoma confined to the right testis (pT1) in a 26-year-old man. (*A*) Sagittal T2-weighted image shows heterogeneous intratesticular tumor (*arrow*) surrounded by a rim of normal testicular parenchyma. (*B*) Axial T1-weighted image depicts small hyperintense area within the mass (*arrowhead*), corresponding to area of hemorrhage. (*C*) Coronal DCE image shows strong, heterogeneous tumor enhancement (*arrow*). Imaging findings are suggestive of nonseminomatous tumor.
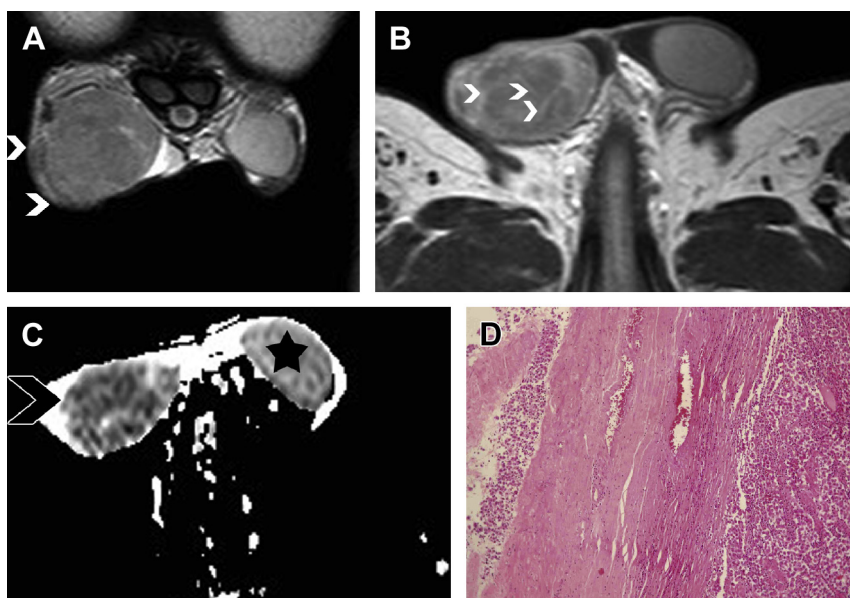

Fig. 7. Right testicular seminoma in a 31-year-old man with invasion of the testicular tunicae (pT2). (*A*) Coronal T2-weighted image depicts large right testicular tumor, invading the testicular tunicae and extending to the paratesticular space (*arrowheads*). The neoplasm is homogeneous and hypointense. (*B*) Axial postcontrast T1-weighted image shows tumor septa (*arrowheads*) enhancing more than the remaining tissue. Imaging findings are suggestive of a seminomatous lesion. (*C*) Transverse ADC map ($b = 900$ s/mm^{-2}) shows tumor hypointensity (*arrowhead*). The ADC values of testicular seminoma are 0.52×10^{-3} mm^2/s^{-1}. The ADC values of the normal contralateral testis (*asterisk*) are 0.85×10^{-3} mm^2/s^{-1}. (*D*) Histologic section (hematoxylin-eosin, original magnification $\times$ 100). Seminoma of the testis: the tumor cells infiltrate the capsule.
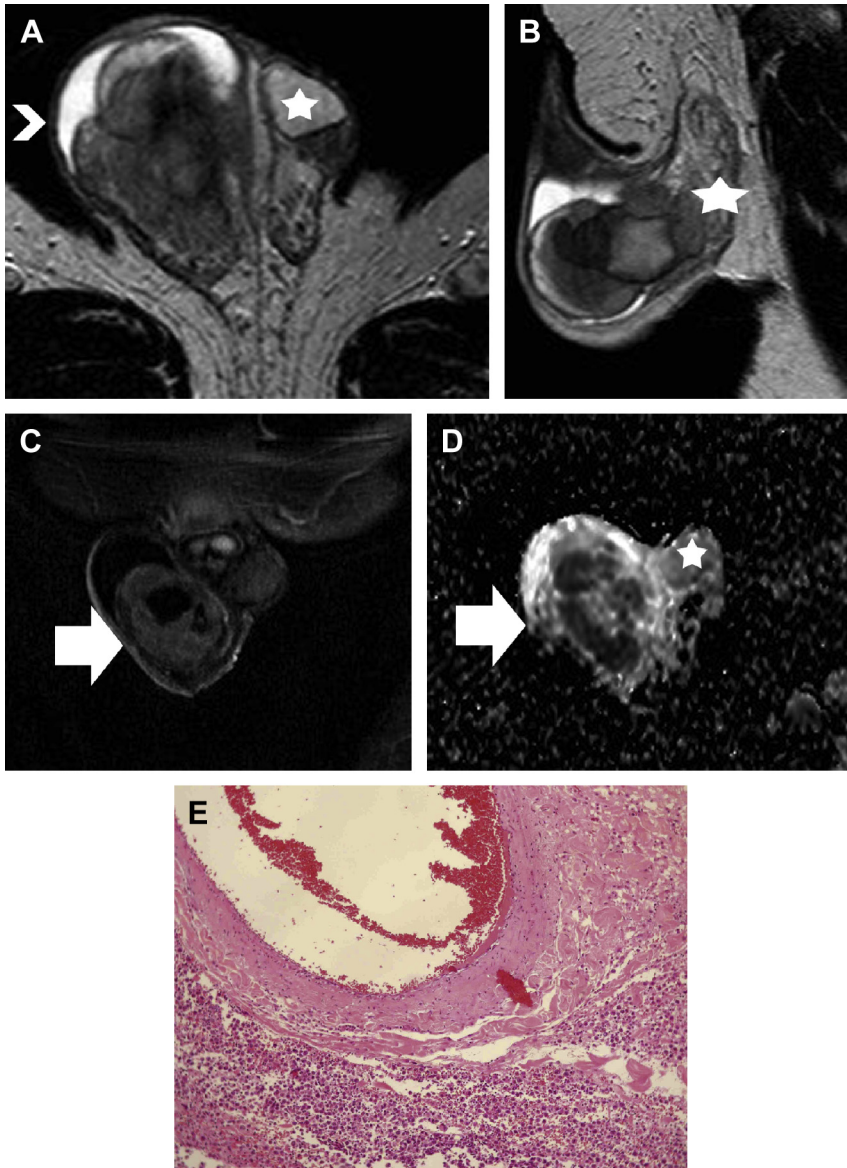
Fig. 8. Right testicular seminoma in a 41-year-old man with Down syndrome, invading the spermatic cord (pT3). (*A*) Transverse and (*B*) sagittal T2-weighted image reveals a large, heterogeneous, mainly hypointense right intra-testicular mass, extending into the proximal part of the spermatic cord (*asterisk*, *B*). Small right hydrocele (*arrow-head*). Atrophic left testis (*asterisk*, *A*). (*C*) Coronal DCE image at an early phase (180 seconds) shows strong, inhomogeneous tumor enhancement (*arrow*). (*D*) Transverse ADC map ($b = 900$ s/mm^{-2}) shows tumor hypointensity (*arrow*). The ADC values of testicular carcinoma are 0.65×10^{-3} mm^2/s^{-1}. The ADC values of the contralateral testis (*asterisk*) are 1.42×10^{-3} mm^2/s^{-1}. (*E*) Histologic section (hematoxylin-eosin, original magnification $\times$ 100). Seminoma of the testis: the neoplastic cells infiltrate the seminiferous duct.

bands, usually infiltrated by lymphocytes and plasma cells.[96] Therefore, on MR imaging, seminomas are often depicted as multinodular tumors of uniform signal intensity, hypointense on T2-weighted sequences. Bandlike structures of low signal intensity on T2-weighted images, enhancing more than the remaining tumor tissue after gadolinium administration, are often seen within these neoplasms, corresponding to the fibro-vascular septa (**Fig. 9**).[18,34] NSGCTs have extremely diverse histologic characteristics and, therefore, are expected to appear as heterogeneous masses on MR imaging, with areas of hemorrhage and/or necrosis, showing inhomogeneous
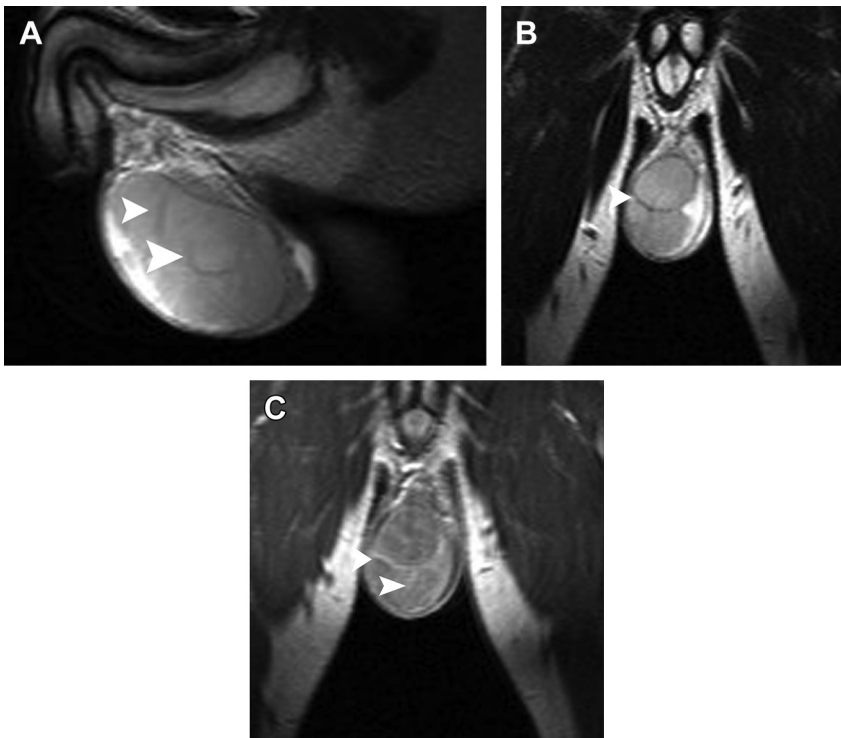
Fig. 9. Typical right testicular seminoma, confined to the testis. Sagittal (*A*) and coronal (*B*) T2-weighted images show multinodular right intratesticular mass. The tumor is mainly hypointense on T2-weighted images, with thin hypointense septa (*arrowheads*). (*C*) Coronal postcontrast T1-weighted image shows enhancement of tumor septa (*arrowheads*). Imaging findings are suggestive of seminomatous tumor.

enhancement after gadolinium administration (see **Figs. 5** and **6**). A hypointense halo on T2-weighted images may be detected at the periphery of testicular tumors, more often in NSGCTs, corresponding to a fibrous capsule on histology (see **Fig. 5**). Based on MR imaging findings, differentiation between seminomatous from nonseminomatous tumors was possible in 91% of cases in a retrospective review of 21 GCTs.[18]

On DCE MR imaging, testicular carcinomas usually show an early upstroke, followed by gradual washout of the contrast medium (type III curve, **Figs. 10** and **11**).[62–64] Testicular malignancies are often hyperintense on DW images, when compared with the usually hypointense benign scrotal lesions and even to the normally hyperintense testicular parenchyma.[70] The ADC values ($\times 10^{-3}$ mm^2/s) of intratesticular malignancies (0.85 $\pm$ 0.62) are lower than that of normal testicular parenchyma and benign intratesticular lesions (see **Figs. 4**E, **7C**, and **8D**).[70] Restricted diffusion in testicular malignancies is mainly related to high tumor cellularity, densely packed neoplastic cells, and enlargement of the nuclei, all resulting in reduced mobility of water molecules.[70]

MR imaging has been reported useful in the preoperative evaluation of the local stage T in testicular carcinomas, which is particularly recommended in cases of planned TSS. The preoperative knowledge of the exact tumor dimensions, possible invasion of the rete testis or the paratesticular space and the presence of a pseudocapsule facilitating possible tumor enucleation are extremely important. According to a retrospective study of 28 testicular tumors, the local extension of testicular carcinomas evaluated by MR imaging was in agreement with the histopathologic findings in 92.8% of cases.[17] The MR imaging criteria used to assess the local extent of testicular cancer are presented in **Table 3** and some examples are given in **Figs. 4–8**.

The preoperative characterization of sex cord and stromal testicular tumors based on imaging findings is usually difficult.[12] However, benign Sertoli cell tumors have been reported as relatively homogeneous hypointense intratesticular masses on T2-weighted sequences, homogeneously enhancing after gadolinium administration, with a very fast early contrast enhancement, followed by rapid washout of the contrast medium (type III
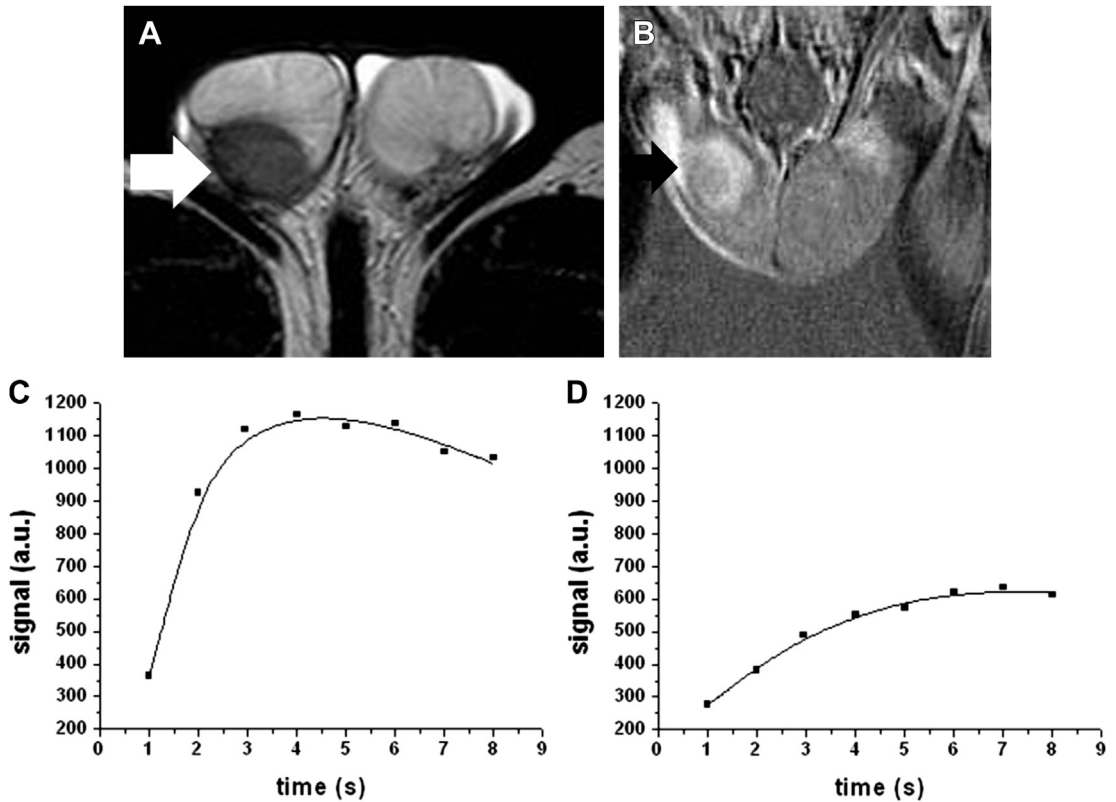
Fig. 10. Classic right testicular seminoma in a 31-year-old man. (*A*) Transverse T2-weighted image shows homogeneous, hypointense right testicular tumor (*arrow*). (*B*) Coronal DCE subtracted image at early (180 seconds) phase shows strong, heterogeneous lesion enhancement (*arrow*). (*C*) TSI plot of the neoplasm depicts avid, early contrast enhancement, followed by gradual de-enhancement (type III). (*D*) TSI plot of the normal contralateral testis (type I).

curve).[62,64,70] Diffusion imaging is useful in the differential diagnosis between Sertoli cell tumors and GCTs. Sertoli cell tumors present less restricted diffusion than GCTs.

Imaging findings of lymphomatous or leukemic infiltration of testicular parenchyma is usually nonspecific. However, the diagnosis of primary testicular lymphoma may be suggested in the presence of a hypointense intratesticular mass on T2-weighted sequences, strongly and heterogeneously enhancing after gadolinium administration, and detected in a men older than 60 years (**Fig. 12**).[94]

Benign Intratesticular Masses

Although rare, benign intratesticular mass lesions, including tubular ectasia of rete testis (TERT), epidermoid cyst, testicular infarction, fibrosis, hematoma, testicular hemorrhagic necrosis, and orchitis, should be accurately characterized to avoid unnecessary radical orchiectomy. MR imaging of the scrotum provides satisfactory results in

the differential diagnosis between benign and malignant intratesticular masses.[12,15–17] Serra and colleagues[16] reported an overall accuracy of 91% in the characterization of intratesticular lesions after inconclusive clinical and sonographic findings. In the researchers' report, MR imaging shows a high sensitivity (100%), specificity (87.5%), and accuracy (96.4%) in differentiating intratesticular masses.[17] Absence of contrast enhancement proved to be the most sensitive sign for predicting the benign nature of intratesticular masses (**Figs. 13–16**).[17] However, benign intratesticular lesions may enhance. In these cases, DCE MR imaging or DW sequences may add valuable information in the differential diagnosis.[62] Benign intratesticular masses usually exhibit strong enhancement, with a late peak, followed by either a plateau or a gradual increase of signal intensity in the delayed phase on DCE MR imaging (type II curve, **Fig. 17**).[62] No restricted diffusion and a mean ADC value ($\times 10^{-3}$ mm^2/s) of 1.56 ± 0.85 have been reported for benign intratesticular mass lesions (**Fig. 18**).[70]
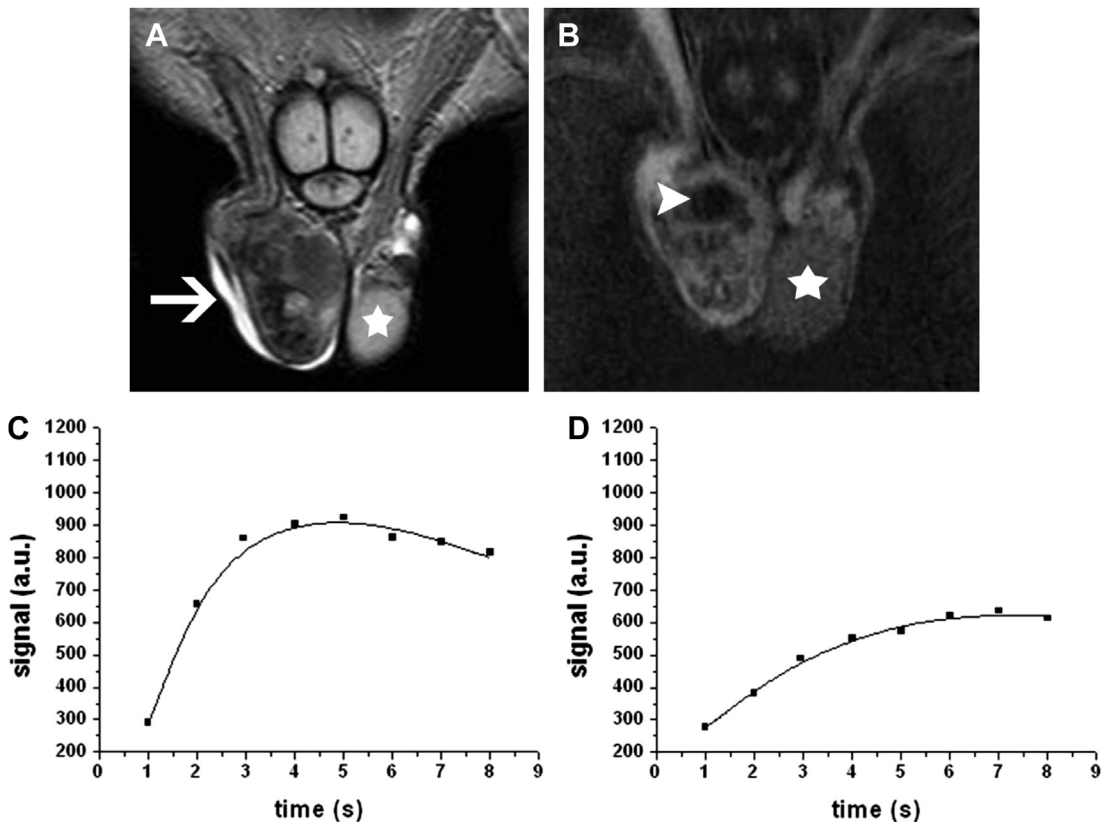
Fig. 11. Mixed germ cell tumor (embryonal carcinoma, seminoma, yolk sac tumor, and teratoma) of the right testis in a 27-year-old man. (*A*) Coronal T2-weighted image depicts heterogeneous right testicular mass, replacing the testis. Small right hydrocele (*arrow*). The contralateral normal testis (*asterisk*) enhances moderately and homogeneously. (*B*) Coronal DCE subtracted image at late (360 seconds) phase shows heterogeneous tumor enhancement, with an area of necrosis (*arrowhead*). (*C*) TSI curve of the neoplasm is suggestive of malignancy (type III). (*D*) TSI curve of the normal contralateral testis (type I).

Table 3 MR imaging criteria for local stage T of testicular cancer	
Stage of Primary Tumor	**Extent of Primary Tumor Assessed on MR Imaging**
pT1	Intratesticular tumor surrounded by a rim of normal testicular parenchyma and/or intact testicular tunicae, detected as a continuous hypointense halo in the periphery of the testis
pT2	Intratesticular tumor invading the testicular tunicae, with or without presence of mass in the paratesticular space
pT3	Enlargement and contrast-enhancement of the spermatic cord because of tumor extension
pT4	Invasion of the scrotal wall by tumor

TERT is a relatively common benign condition, which may mimic neoplasia, both clinically and sonographically.[12,17,55,56] The MR imaging findings are typical, including multicystic masses of variable size, with signal intensity similar to that of water, free diffusion, and lack of contrast enhancement (see **Fig. 13**). TERT is typically located in the mediastinum testis and it is often bilateral.[55,56]

Epidermoid cysts account for approximately 1% of all testicular masses.[12] Pathologically, it is composed of concentric layers of laminated keratinous material, which produce a characteristic target appearance on imaging. The typical MR imaging finding includes the presence of alternating zones of high and low signal intensity on T2-weighted images, corresponding to both high water and lipid content and dense keratin debris and calcifications, respectively, on pathology. Absence of contrast enhancement confirms the benignity of the lesion (see **Fig. 14**).[52–54]
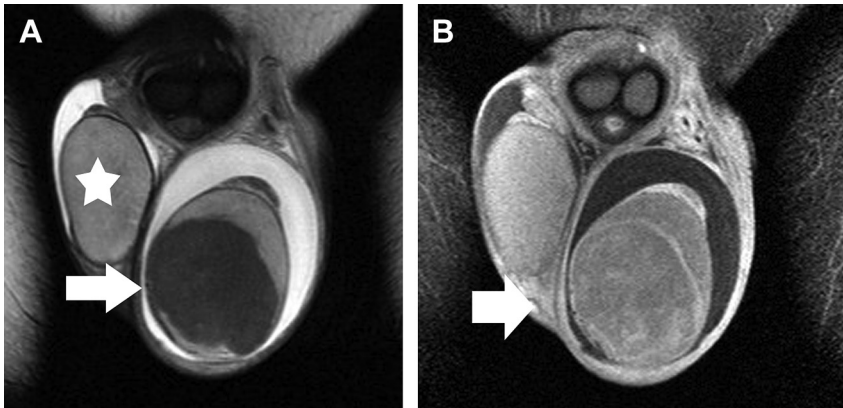
Fig. 12. Primary diffuse large B-cell testicular lymphoma in a 52-year-old man. Coronal (*A*) T2- and (*B*) contrast-enhanced T1-weighted images depict large left intratesticular mass lesion (*arrow*). The tumor is mainly hypointense on T2-weighted images, when compared with the normal contralateral testis (*asterisk*, *A*) and enhances heterogeneously. A moderate left hydrocele and a small right hydrocele are also noted.

Testicular fibrosis may mimic malignancy on sonographic examination. The MR imaging findings suggesting the diagnosis of testicular fibrosis are the presence of an intratesticular mass with a low on T1-weighted signal intensity and a very low T2-weighted signal intensity, not enhancing after gadolinium administration.[15–17]

Segmental testicular infarction is an infrequent testicular disease.[57] The presence of a triangular-shaped avascular intratesticular mass lesion on MR imaging, pointing toward the rete testis, hypointense on T2-weighted images, with a surrounding markedly enhancing rim may strongly suggest testicular infarction.[57] A hyperintense testis on T1-weighted images, with a very low signal intensity or with a spotty or streaked pattern of very low signal intensity on T2-weighted images and decreased or absent enhancement after

contrast administration, is suggestive of hemorrhagic necrosis of the testicle (see **Fig. 15**).[17,66]

Scrotal inflammatory disease may mimic neoplasia in all phases of evolution, especially in chronic stages. It is considered the most common cause of false-positive scrotal explorations. Isolated granulomatous orchitis is a rare disease, with obscure pathogenesis.[12] Absence of contrast enhancement and restricted diffusion may be useful for considering the benign nature of this entity (see **Fig. 16**).[41]

Paratesticular Masses

MR imaging allows precise localization of scrotal masses and defines the anatomic relationship to the surrounding structures (**Fig. 19**). Most paratesticular mass lesions are benign, including cysts

Fig. 13. Bilateral tubular ectasia of the rete testis in a 64-year-old man. (*A*) Transverse T2-weighted image shows multilocular intratesticular lesions (*arrowheads*), located in the mediastinum. The lesions have signal intensity similar to that of water. A right spermatocele (*arrow*) is also noted. Small hydrocele is seen bilaterally (physiologic finding). (*B*) Coronal DCE image depicts absence of enhancement of the right intratesticular lesion (*arrowhead*). (*C*) Transverse ADC map ($b = 900$ s/mm^{-2}). The ADC values of the normal testes are 1.30×10^{-3} mm^2/s^{-1} (*right*) and 1.32×10^{-3} mm^2/s^{-1} (*left*). Tubular ectasia of rete testis appears hyperintense on the ADC maps (*arrowheads*), with an ADC value of 2.5×10^{-3} mm^2/s^{-1} (*right*) and 2.66×10^{-3} mm^2/s^{-1} (*left*).
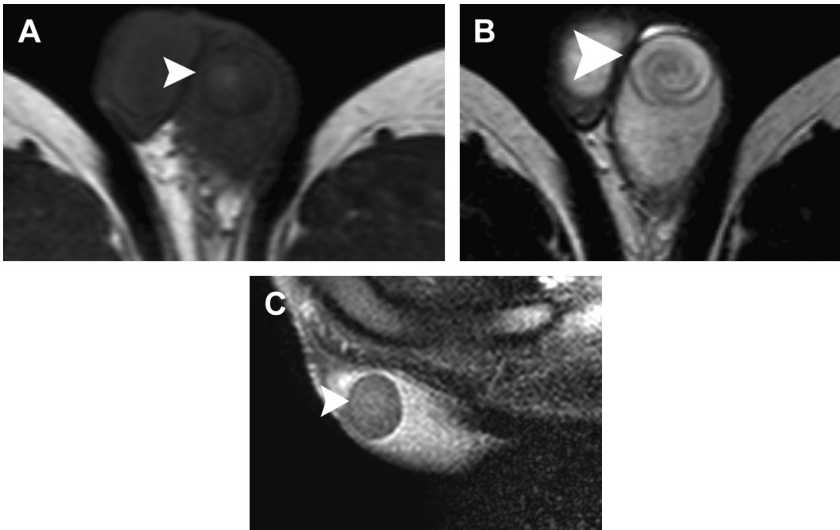
Fig. 14. Epidermoid cyst of the left testis in a 20-year-old man. (*A*) Transverse T1-weighted image shows a left intratesticular mass lesion, with smooth margins and a hyperintense area centrally (*arrowhead*), corresponding to dense keratinized material and calcifications on histology. (*B*) Transverse T2-weighted image depicts the typical onion-skin appearance of the lesion (*arrowhead*), corresponding to the laminated layers of keratinized material on pathology. Imaging findings were suggestive of an epidermoid cyst diagnosis. (*C*) Sagittal fat-suppressed T1-weighted image after gadolinium administration shows absence of lesion enhancement (*arrowhead*), a finding suggestive of benignity.
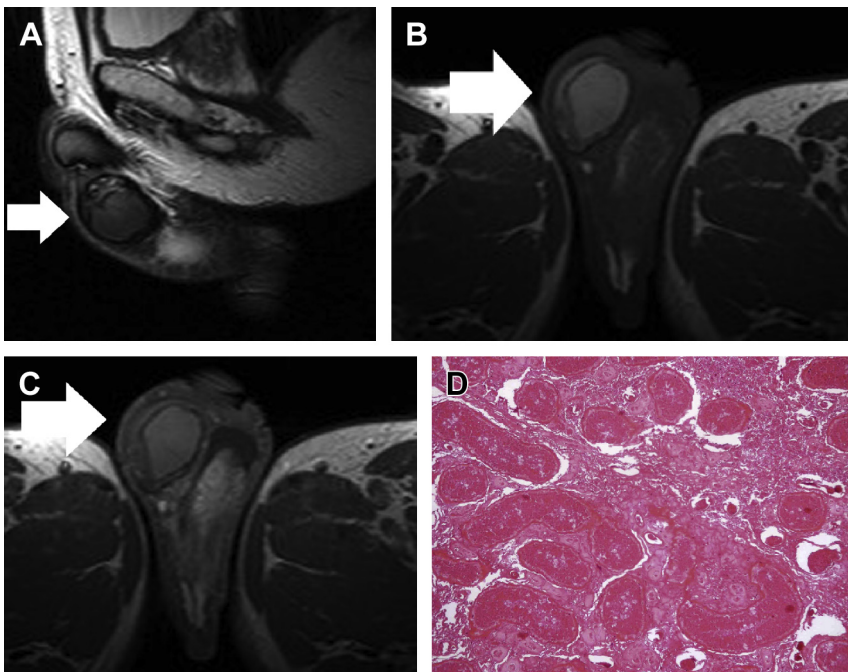

Fig. 15. Right testicular hemorrhagic necrosis in a 56-year-old man. (*A*) Sagittal T2-weighted image depicts right testis with very low signal intensity (*arrow*). (*B*) Transverse T1-weighted image demonstrates hyperintensity of right testis (*arrow*). (*C*) Transverse T1-weighted image after gadolinium administration depicts lack of enhancement of the right testis (*arrow*). (*D*) Histologic section (hematoxylin-eosin, original magnification × 100): ghost seminiferous tubules.
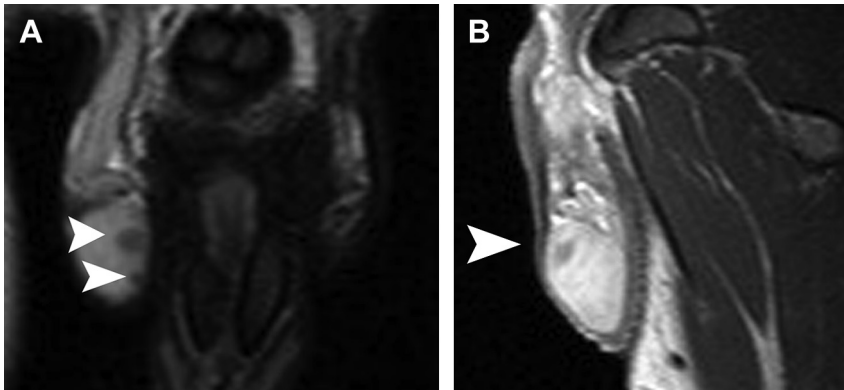
Fig. 16. Granulomatous orchitis in a 33-year-old man. (*A*) Coronal T2-weighted image depicts 2 small-sized right intratesticular mass lesions (*arrowheads*), mainly hypointense. (*B*) Sagittal postcontrast T1-weighted image shows absence of contrast enhancement (*arrowhead*), a finding suggestive of a benign diagnosis.
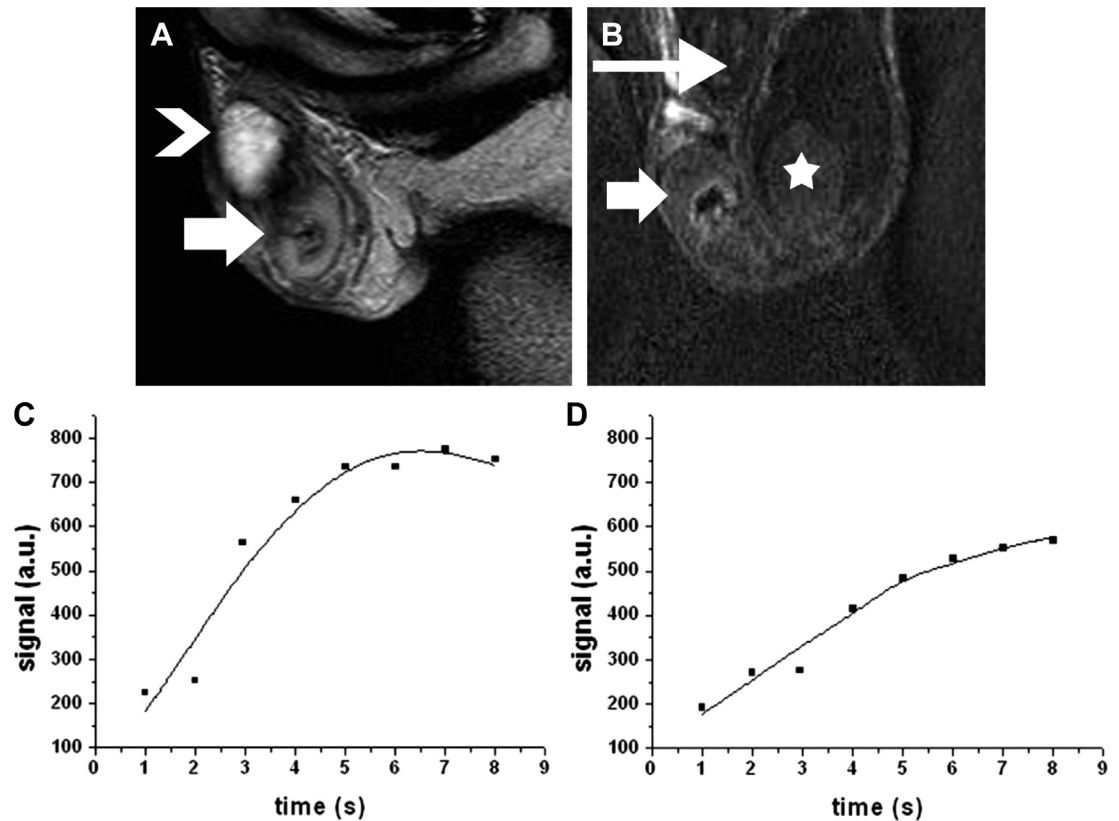

Fig. 17. Postbiopsy changes of the right testis in a 36-year-old man. Histology was negative for malignancy. (*A*) Sagittal T2-weighted image depicts heterogeneous mass lesion in the lower pole of the right testis (*arrow*). A moderate amount of hydrocele (*arrowhead*) is seen in the left hemiscrotum. (*B*) Coronal DCE subtracted image at early (180 seconds) phase demonstrates strong, heterogeneous lesion enhancement (*arrow*). Left testis (*asterisk*) enhances homogeneously. Left hydrocele (*long arrow*). (*C*) TSI curve of the intratesticular mass lesion shows an initial upstroke, followed by a plateau in the late postcontrast phase (type II). (*D*) TSI curve of the normal left testis depicts a moderate, linear increase of contrast enhancement throughout the examination (type I).
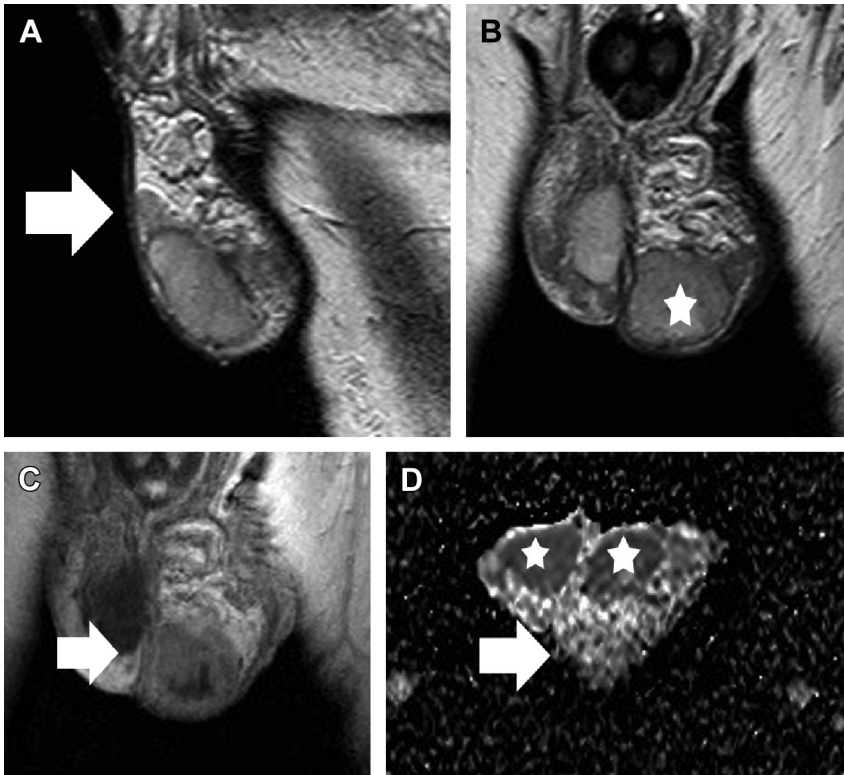
Fig. 18. Left epididymo-orchitis in a 71-year-old man. (*A*) Sagittal and (*B*) coronal T2-weighted images show enlargement and hypointensity of both the left epididymis (*arrow, A*) and the testis (*asterisk, B*). (*C*) Coronal DCE image depicts heterogeneous lesion enhancement (*arrow*). (*D*) The ADC values of the left epididymis (*arrow*) are 1.53×10^{-3} mm^2/s and that of the ipsilateral testis (*asterisk*) 0.94×10^{-3} mm^2/s, (right testis: 1.05×10^{-3} mm^2/s, *asterisk*).

and spermatoceles; scrotal fluid collections, like hydroceles and pyoceles; inflammatory lesions; and hernias.[13] In epididymitis/epididymo-orchitis, MR imaging shows a slightly high signal on T2-weighted images, increased diffusion, and inhomogeneous enhancement (see **Fig. 18**; **Fig. 20**).

Solid neoplasms of the paratesticular space are rare.[13,14,43–49,88,89] They may occur at all ages, usually presenting as slow-growing painless scrotal masses. The preoperative characterization of paratesticular tumors may be difficult. In some cases, however, MR imaging findings, in combination with tumor location, morphology, and tissue characteristics, may help to narrow the differential diagnosis. DWI may further help for lesion characterization.[70] Hypointensity on DWI and increased ADC ($1.72 \pm 0.60 \times 10^{-3}$ mm^2/s) is in favor of benign paratesticular lesions.[70]

Lipoma is the most common benign tumor of the paratesticular space, usually arising from the spermatic cord. The tumor is readily identified on MR imaging, owing to its characteristic signal intensity, high and low on T1 and fat-suppressed T1-weighted images, respectively.[13] Adenomatoid

tumor is the most common tumor of the epididymis, followed by leiomyoma.[13,48,49] Patel and Silva[49] described the MR imaging findings of an adenomatoid tumor of the tunica albuginea, appearing as a slightly hypointense mass on unenhanced T1-weighted images, enhancing after gadolinium administration.

Other rare benign paratesticular tumors include fibroma, hemangioma, neurofibroma, and papillary cystadenoma.[13] Fibrous pseudotumor is not a true neoplasm but rather a reactive proliferation of paratesticular tissue. Approximately 75% of cases arise from the tunica vaginalis and the rest from the epididymis, the spermatic cord, or the tunica albuginea. MR imaging may enable its correct characterization, as the lesion appears with low signal intensity on both T1- and T2-weighted sequences because of the fibrous tissue content.[13,43–47]

In adults, the differential diagnosis of paratesticular masses should also include malignancies, like leiomyosarcoma, fibrosarcoma, liposarcoma, and lymphoma. These neoplasms are extremely rare. Finally, metastases, most commonly from
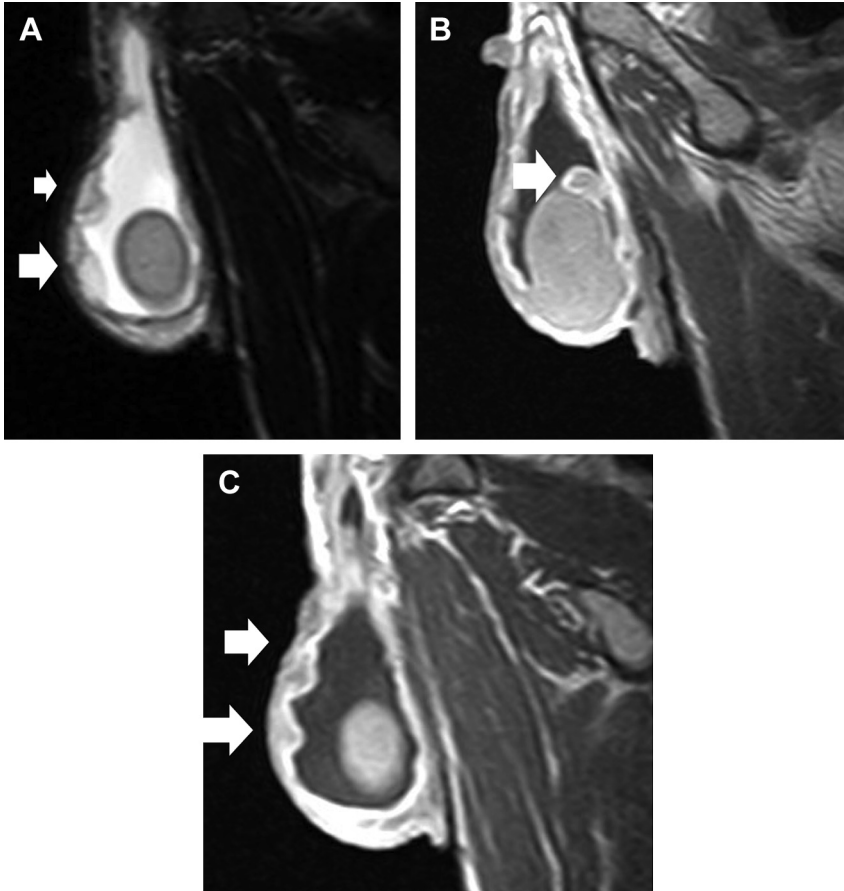
Fig. 19. Paratesticular metastases from low-grade adenocarcinoma in a 54-year-old man. Sagittal (*A*) T2 and (*B*, *C*) fat-suppressed postcontrast T1-weighted images show large right hydrocele and multiple nodular small-sized masses in the paratesticular space (*arrows*). The lesions have signal intensity similar to that of normal testis on T2-weighted image and enhance strongly after gadolinium administration.
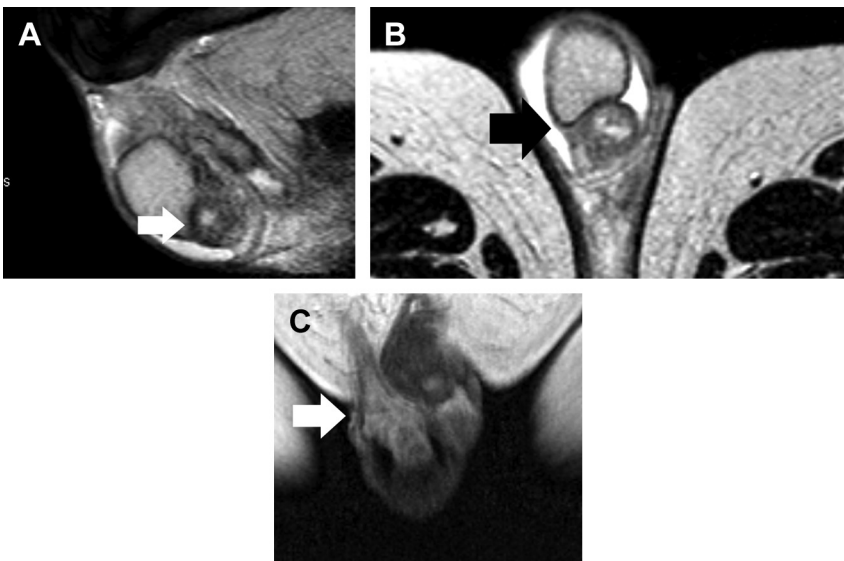

Fig. 20. Right epididymitis in a 79-year-old man. (*A*) Sagittal and (*B*) transverse T2-weighted images show enlargement and heterogeneity of the right epididymal tail (*arrow*). (*C*) Coronal DCE depicts heterogeneous enhancement of the right epididymal head (*arrow*). Imaging findings are typical of epididymitis.

testicular, prostatic, renal, and gastrointestinal primary neoplasms, should be considered, especially if there is a history of primary tumor (see **Fig. 19**).[13]

FUTURE CONSIDERATIONS/SUMMARY

Imaging of the scrotum has experienced significant advancements during the last few years. The goal is to improve the diagnosis and management of men with acute scrotal disease or a palpable mass and to reduce the number of unnecessary radical orchiectomies. Contrast-enhanced sonography has been proposed as an alternative modality in cases of inconclusive sonographic findings.[97–100] MR imaging of the scrotum, although it cannot be considered the first imaging technique in the investigation of scrotal diseases, has been proved an efficient diagnostic tool for scrotal imaging. Functional MR imaging techniques, including DCE MR imaging, DWI, and MRS, may provide additional diagnostic information in the interpretation of scrotal diseases. Large prospective studies directly comparing the diagnostic performances of sonography and MR imaging might justify the role of MR imaging in the investigation of scrotal diseases.

REFERENCES

1. Dogra VS, Gottlieb RH, Oka M, et al. Sonography of the scrotum. Radiology 2003;227(1):18–36.
2. Bhatt S, Dogra VS. Role of US in testicular and scrotal trauma. Radiographics 2008;28(6):1617–29.
3. Dogra V, Bhatt S. Acute painful scrotum. Radiol Clin North Am 2004;42(2):349–63.
4. Bhatt S, Rubens DJ, Dogra VS. Sonography of benign intrascrotal lesions. Ultrasound Q 2006;22(2):121–36.
5. Hamm B. Differential diagnosis of scrotal masses by ultrasound. Eur Radiol 1997;7(5):668–79.
6. Hamm B. Sonography of the testis and epididymis. Andrologia 1994;26(4):193–210.
7. Pavlica P, Barozzi L. Imaging of the acute scrotum. Eur Radiol 2001;11(2):220–8.
8. Tessler FN, Tublin ME, Rifkin MD. Ultrasound assessment of testicular and paratesticular masses. J Clin Ultrasound 1996;24(8):423–36.
9. Aganovic L, Cassidy F. Imaging of the scrotum. Radiol Clin North Am 2012;50(6):1145–65.
10. Cassidy FH, Ishioka KM, McMahon CJ, et al. MR imaging of scrotal tumors and pseudotumors. Radiographics 2010;30(3):665–83.
11. Mohrs OK, Thoms H, Egner T, et al. MRI of patients with suspected scrotal or testicular lesions: diagnostic value in daily practice. AJR Am J Roentgenol 2012;199(3):609–15.
12. Woodward PJ, Sohaey R, O'Donoghue MJ, et al. Tumors and tumorlike lesions of the testis: radiologic-pathologic correlation. Radiographics 2002;22(1):189–216.
13. Akbar SA, Sayyed TA, Jafri SZ, et al. Multimodality imaging of paratesticular neoplasms and their rare mimics. Radiographics 2003;23(6):1461–76.
14. Woodward PJ, Schwab CM, Sesterhenn IA. Extra-testicular scrotal masses: radiologic-pathologic correlation. Radiographics 2003;23(1):215–40.
15. Muglia V, Tucci S Jr, Elias J Jr, et al. Magnetic resonance imaging of scrotal diseases: when it makes the difference. Urology 2002;59(3):419–23.
16. Serra AD, Hricak H, Coakley FV, et al. Inconclusive clinical and ultrasound evaluation of the scrotum: impact of magnetic resonance imaging on patient management and cost. Urology 1998;51(6):1018–21.
17. Tsili AC, Argyropoulou MI, Giannakis D, et al. Magnetic resonance imaging in the characterization and local staging of testicular neoplasms. AJR Am J Roentgenol 2010;194(3):682–9.
18. Tsili AC, Tsampoulas C, Giannakopoulos X, et al. MRI in the histologic characterization of testicular neoplasms. AJR Am J Roentgenol 2007;189(6):W331–7.
19. Mattrey RF. Magnetic resonance imaging of the scrotum. Semin Ultrasound CT MR 1991;12(2):95–108.
20. Schnall M. Magnetic resonance imaging of the scrotum. Semin Roentgenol 1993;28(1):19–30.
21. Seidenwurm D, Smathers RL, Lo RK, et al. Testes and scrotum: MR imaging at 1.5 T. Radiology 1987;164(2):393–8.
22. Baker LL, Hajek PC, Burkhard TK, et al. MR imaging of the scrotum: normal anatomy. Radiology 1987;163(1):89–92.
23. Baker LL, Hajek PC, Burkhard TK, et al. MR imaging of the scrotum: pathologic conditions. Radiology 1987;163(1):93–8.
24. Rholl KS, Lee JK, Ling D, et al. MR imaging of the scrotum with a high-resolution surface coil. Radiology 1987;163(1):99–103.
25. Fritzsche PJ. MRI of the scrotum. Urol Radiol 1988;10(1):52–7.
26. Schultz-Lampel D, Bogaert G, Thüroff JW, et al. MRI for evaluation of scrotal pathology. Urol Res 1991;19(5):289–92.
27. Thurnher S, Hricak H, Carroll PR, et al. Imaging the testis: comparison between MR imaging and US. Radiology 1988;167(3):631–6.
28. Sohn M, Neuerburg J, Bohndorf K, et al. The value of magnetic resonance imaging at 1.5 T in the evaluation of the scrotal content. Urol Int 1989;44(5):284–91.
29. Sica GT, Teeger S. MR imaging of scrotal, testicular, and penile diseases. Magn Reson Imaging Clin N Am 1996;4(3):545–63.

30. Andipa E, Liberopoulos K, Asvestis C. Magnetic resonance imaging and ultrasound evaluation of penile and testicular masses. World J Urol 2004; 22(5):382–91.

31. Cramer BM, Schlegel EA, Thueroff JW. MR imaging in the differential diagnosis of scrotal and testicular disease. Radiographics 1991;11(1):9–21.

32. Müller-Leisse C, Bohndorf K, Stargardt A, et al. Gadolinium-enhanced T1-weighted versus T2-weighted imaging of scrotal disorders: is there an indication for MR imaging? J Magn Reson Imaging 1994;4(3):389–95.

33. Mäkelä E, Lahdes-Vasama T, Ryymin P, et al. Magnetic resonance imaging of acute scrotum. Scand J Surg 2011;100(3):196–201.

34. Johnson JO, Mattrey RF, Phillipson J. Differentiation of seminomatous from nonseminomatous testicular tumors with MR imaging. AJR Am J Roentgenol 1990;154(3):539–43.

35. Bhatt S, Jafri SZ, Wassermann N, et al. Imaging of non-neoplastic intratesticular masses. Diagn Interv Radiol 2011;17(1):52–63.

36. Sohaib SA, Koh DM, Husband JE. The role of imaging in the diagnosis, staging, and management of testicular cancer. AJR Am J Roentgenol 2008; 191(2):387–95.

37. Fütterer JJ, Heijmink SW, Spermon JR. Imaging the male reproductive tract: current trends and future directions. Radiol Clin North Am 2008; 46(1):133–47.

38. Fritzsche PJ, Hricak H, Kogan BA, et al. Undescended testis: value of MR imaging. Radiology 1987;164(1):169–73.

39. Kier R, McCarthy S, Rosenfield AT, et al. Nonpalpable testes in young boys: evaluation with MR imaging. Radiology 1988;169(2):429–33.

40. Miyano T, Kobayashi H, Shimomura H, et al. Magnetic resonance imaging for localizing the nonpalpable undescended testis. J Pediatr Surg 1991; 26(5):607–9.

41. Tsili AC, Argyropoulou MI, Giannakis D, et al. Isolated granulomatous orchitis: MR imaging findings. Eur J Radiol Extra 2011;79(2):e81–3.

42. Trambert MA, Mattrey RF, Levine D, et al. Subacute scrotal pain: evaluation of torsion versus epididymitis with MR imaging. Radiology 1990; 175(1):53–6.

43. Ch Tsili A, Tsampoulas C, Giannakopoulos X, et al. Solitary fibrous tumor of the epididymis: MRI features. Br J Radiol 2005;78(930):565–8.

44. Grebenc ML, Gorman JD, Sumida FK. Fibrous pseudotumor of the tunica vaginalis testis: imaging appearance. Abdom Imaging 1995;20(4):379–80.

45. Saginoya T, Yamaguchi K, Toda T, et al. Fibrous pseudotumor of the scrotum: MR imaging findings. AJR Am J Roentgenol 1996;167(1):285–6.

46. Krainik A, Sarrazin JL, Camparo P, et al. Fibrous pseudotumor of the epididymis: imaging and pathologic correlation. Eur Radiol 2000;10(10): 1636–8.

47. Tobias-machado M, Corrêa Lopes Neto A, Heloisa Simardi L, et al. Fibrous pseudotumor of tunica vaginalis and epididymis. Urology 2000;56(4): 670–2.

48. Tsili AC, Argyropoulou MI, Giannakis D, et al. Conventional and diffusion-weighted magnetic resonance imaging findings of benign fibromatous paratesticular tumor: a case report. J Med Case Rep 2011;3(5):169.

49. Patel MD, Silva AC. MRI of an adenomatoid tumor of the tunica albuginea. AJR Am J Roentgenol 2004;182(2):415–7.

50. Tsili AC, Tsampoulas C, Giannakis D, et al. Tuberculous epididymo-orchitis: MRI findings. Br J Radiol 2008;81(966):e166–9.

51. Baker LL, Hajek PC, Burkhard TK, et al. Polyorchidism: evaluation by MR. AJR Am J Roentgenol 1987; 148(2):305–6.

52. Loya AG, Said JW, Grant EG. Epidermoid cyst of the testis: radiologic-pathologic correlation. Radiographics 2004;24(Suppl 1):S243–6.

53. Cho JH, Chang JC, Park BH, et al. Sonographic and MR imaging findings of testicular epidermoid cysts. AJR Am J Roentgenol 2002;178(3):743–8.

54. Langer JE, Ramchandani P, Siegelman ES, et al. Epidermoid cysts of the testicle: sonographic and MR imaging features. AJR Am J Roentgenol 1999;173(5):1295–9.

55. Rouviere O, Bouvier R, Pangaud C, et al. Tubular ectasia of the rete testis: a potential pitfall in scrotal imaging. Eur Radiol 1999;9(9):1862–8.

56. Tartar VM, Trambert MA, Balsara ZN, et al. Tubular ectasia of the testicle: sonographic and MR imaging appearance. AJR Am J Roentgenol 1993; 160(3):539–42.

57. Fernández-Pérez GC, Tardáguila FM, Velasco M. Radiologic findings of segmental testicular infarction. AJR Am J Roentgenol 2005;184(5):1587–93.

58. Albers P, Albrecht W, Algaba F, et al. European Association of Urology. Guidelines on testicular cancer. Updates 2011. Available at: http://www. uroweb.org/gls/pdf/11_Testicular_Cancer_LR.pdf. Accessed July 20, 2013.

59. Krege S, Beyer J, Souchon R, et al. European consensus conference on diagnosis and treatment of germ cell cancer: a report of the second meeting of the European Germ Cell Cancer Consensus Group (EGCCCG): part I. Eur Urol 2008;53(3): 478–96.

60. Krege S, Beyer J, Souchon R, et al. European consensus conference on diagnosis and treatment of germ cell cancer: a report of the second meeting of the European Germ Cell Cancer Consensus

Group (EGCCCG): part II. Eur Urol 2008;53(3): 497–513.

61. Giannarini G, Dieckmann KP, Albers P, et al. Organ-sparing surgery for adult testicular tumours: a systematic review of the literature. Eur Urol 2010; 57(5):780–90.

62. Tsili AC, Argyropoulou MI, Astrakas LG, et al. Dynamic contrast-enhanced subtraction MRI for characterizing intratesticular mass lesions. AJR Am J Roentgenol 2013;200(3):578–85.

63. Watanabe Y, Dohke M, Ohkubo K, et al. Scrotal disorders: evaluation of testicular enhancement patterns at dynamic contrast-enhanced subtraction MR imaging. Radiology 2000;217(1): 219–27.

64. Reinges MH, Kaiser WA, Miersch WD, et al. Dynamic MRI of benign and malignant testicular lesions: preliminary observations. Eur Radiol 1995; 5(6):615–22.

65. Reinges MH, Kaiser WA, Miersch WD, et al. Dynamic magnetic resonance imaging of the contralateral testis in patients with malignant tumor of the testis. Urology 1994;44(4):540–7.

66. Watanabe Y, Nagayama M, Okumura A, et al. MR imaging of testicular torsion: features of testicular hemorrhagic necrosis and clinical outcomes. J Magn Reson Imaging 2007;26(1):100–8.

67. Terai A, Yoshimura K, Ichioka K, et al. Dynamic contrast-enhanced subtraction magnetic resonance imaging in diagnostics of testicular torsion. Urology 2006;67(6):1278–82.

68. Costabile RA, Choyke PL, Frank JA, et al. Dynamic enhanced magnetic resonance imaging of testicular perfusion in the rat. J Urol 1993;149(5):1195–7.

69. Choyke PL. Dynamic contrast-enhanced MR imaging of the scrotum: reality check. Radiology 2000; 217(1):14–5.

70. Tsili AC, Argyropoulou MI, Giannakis D, et al. Diffusion-weighted MR imaging of normal and abnormal scrotum: preliminary results. Asian J Androl 2012; 14(4):649–54.

71. Kantarci M, Doganay S, Yalcin A, et al. Diagnostic performance of diffusion-weighted MRI in the detection of nonpalpable undescended testes: comparison with conventional MRI and surgical findings. AJR Am J Roentgenol 2010;195(4): W268–73.

72. Kato T, Kojima Y, Shibata Y, et al. Usefulness of MR fat-suppressed T2-weighted and diffusion-weighted imaging for the diagnosis of nonpalpable testes. J Urol 2008;179(4):387–8.

73. Kangasniemi M, Kaipia A, Joensuu R. Diffusion weighted magnetic resonance imaging of rat testes: a method for early detection of ischemia. J Urol 2001;166(6):2542–4.

74. Maki D, Watanabe Y, Nagayama M, et al. Diffusion-weighted magnetic resonance imaging in the detection of testicular torsion: feasibility study. J Magn Reson Imaging 2011;34(5):1137–42.

75. Firat AK, Uğraş M, Karakaş HM, et al. 1H magnetic resonance spectroscopy of the normal testis: preliminary findings. Magn Reson Imaging 2008; 26(2):215–20.

76. Aaronson DS, Iman R, Walsh TJ, et al. A novel application of 1H magnetic resonance spectroscopy: non-invasive identification of spermatogenesis in men with non-obstructive azoospermia. Hum Reprod 2010;25(4):847–52.

77. Yamaguchi M, Mitsumori F, Watanabe H, et al. In vivo localized 1H MR spectroscopy of rat testes: stimulated echo acquisition mode (STEAM) combined with short TI inversion recovery (STIR) improves the detection of metabolite signals. Magn Reson Med 2006;55(4):749–54.

78. Sasagawa I, Tateno T, Yazawa H, et al. Assessment of testicular function in experimental varicocele rats by phophorus-31 magnetic resonance spectroscopy. Urol Res 1998;26(6):407–10.

79. Kiricuta IC, Bluemm RG, Rühl J, et al. 31-P MR spectroscopy and MRI of a testicular non-Hodgkin lymphoma recurrence to monitor response to irradiation. A case report. Strahlenther Onkol 1994;170(6):359–64.

80. Thomsen C, Jensen KE, Giwercman A, et al. Magnetic resonance: in vivo tissue characterization of the testes in patients with carcinoma-in-situ of the testis and healthy subjects. Int J Androl 1987; 10(1):191–8.

81. Paldino MJ, Barboriak DP. Fundamentals of quantitative dynamic contrast-enhanced MR imaging. Magn Reson Imaging Clin N Am 2009; 17(2):277–89.

82. Moon M, Cornfeld D, Weinreb J. Dynamic contrast-enhanced breast MR imaging. Magn Reson Imaging Clin N Am 2009;17(2):351–62.

83. Do RK, Rusinek H, Taouli B. Dynamic contrast-enhanced MR imaging of the liver: current status and future directions. Magn Reson Imaging Clin N Am 2009;17(2):339–49.

84. Schaefer PW, Copen WA, Lev MH, et al. Diffusion-weighted imaging in acute stroke. Magn Reson Imaging Clin N Am 2006;14(2):141–68.

85. de Carvalho Rangel C, Hygino Cruz LC Jr, Takayassu TC, et al. Diffusion MR imaging in central nervous system. Magn Reson Imaging Clin N Am 2011;19(1):23–53.

86. Kim S, Naik M, Sigmund E, et al. Diffusion-weighted MR imaging of the kidneys and the urinary tract. Magn Reson Imaging Clin N Am 2008; 16(4):585–96.

87. American Cancer Society. Cancer facts and figures 2013. Available at: www.cancer.org/acs/groups/content/@epidemiologysurveillance/documents/document/acspc-036845.pdf. Accessed July 20, 2013.

88. Ulbright TM, Amin MB, Young RH. Tumors of the testis, adnexa, spermatic cord and scrotum. In: Rosai J, Sobin LH, editors. Atlas of tumor pathology, fasc 25, ser 3. Washington, DC: Armed Forces Institute of Pathology; 1999. p. 1–290.

89. Ulbright TM, Berney DM. Testicular and paratesticular tumors. In: Mills SE, Carter D, Greenson JK, et al, editors. Sternberg's diagnostic surgical pathology. Philadelphia: Lippincott Williams & Wilkins; 2010. p. 1944–2004.

90. Rosenberg SA. Cancer: principles and practice of oncology. 9th edition. Philadelphia: Lippincott Williams & Wilkins; 2011. p. 1280–301.

91. Woodward PJ, Heidenreich A, Looijenga LH, et al. Germ cell tumours. In: Eble JN, Sauter G, Epstein JI, et al, editors. Pathology and genetics of tumours of the urinary system and male genital organs. Lyon (France): IARC Press; 2004. p. 221–49.

92. Drevelengas A, Kalaitzoglou I, Destouni E, et al. Bilateral Sertoli cell tumor of the testis: MRI and sonographic appearance. Eur Radiol 1999;9(9): 1934.

93. Zicherman JM, Weissman D, Gribbin C, et al. Primary diffuse large B-cell lymphoma of the epididymis and testis. Radiographics 2005;25(1):243–8.

94. Tsili AC, Argyropoulou MI, Giannakis D, et al. Primary diffuse large B-cell testicular lymphoma: magnetic resonance imaging findings. Andrologia 2012;44(Suppl 1):845–7.

95. Liu KL, Chang CC, Huang KH, et al. Imaging diagnosis of testicular lymphoma. Abdom Imaging 2006;31(5):610–2.

96. Rosai J. Rosai and Ackerman's surgical pathology, vol. 1. 10th edition. Philadelphia: Elsevier; 2011. p. 1334–74.

97. Lock G, Schmidt C, Helmich F, et al. Early experience with contrast-enhanced ultrasound in the diagnosis of testicular masses: a feasibility study. Urology 2011;77(5):1049–53.

98. Lung PF, Jaffer OS, Sellars ME, et al. Contrast-enhanced ultrasound in the evaluation of focal testicular complications secondary to epididymitis. AJR Am J Roentgenol 2012;199(3):W345–54.

99. Valentino M, Bertolotto M, Derchi L, et al. Role of contrast enhanced ultrasound in acute scrotal diseases. Eur Radiol 2011;21(9):1831–40.

100. Bertolotto M, Derchi LE, Sidhu PS, et al. Acute segmental testicular infarction at contrast-enhanced ultrasound: early features and changes during follow-up. AJR Am J Roentgenol 2011; 196(4):834–41.